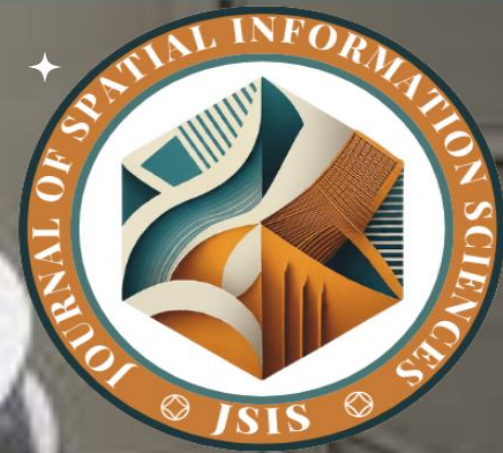


Journal of  
Spatial  
Information  
Sciences

...JSIS



**INVESTIGATING THE ALTITUDE-DEPENDENT  
ACCURACY OF DEPTHS DERIVED BY  
COLOUR RATIO FROM UNMANNED AERIAL  
SYSTEM (UAS)-MULTISPECTRAL  
IMAGERIES**

**Esin Okon, M. N. Ono, Franklin  
Onyeagoro**





## INVESTIGATING THE ALTITUDE-DEPENDENT ACCURACY OF DEPTHS DERIVED BY COLOUR RATIO FROM UNMANNED AERIAL SYSTEM (UAS)-MULTISPECTRAL IMAGERIES

Esin Okon<sup>1\*</sup>, M. N. Ono<sup>2</sup>, Franklin Onyeagoro<sup>3</sup>

<sup>1,2</sup>Department of Surveying and Geoinformatics, Nnamdi Azikiwe University, Awka, Nigeria

<sup>3</sup>Department of Surveying and Geoinformatics, Federal University of Technology, Owerri, Nigeria

\*Correspondence Author: [profesin2000@gmail.com](mailto:profesin2000@gmail.com)

DOI: <https://doi.org/10.5281/zenodo.15668026>

### Abstract:

Bathymetry is an essential requirement in marine applications such as sea navigation, coastal monitoring, forecast of coastal phenomena and engineering constructions. Bathymetry is traditionally acquired via shipboard echo sounding which is usually very expensive, labor-intensive added with inability to access remote or unnavigable areas. But, nowadays, remote sensing methods, such as space-borne or air-borne imaging or lidar have been employed in determining water depth, hence offsetting the setbacks associated with the conventional approaches. Unmanned Aerial System (UAS)-photogrammetry offers a good opportunity for mapping waterbody bottom relief because of its higher image resolution. The study, targeted at determining the various accuracies of bathymetries achievable at two different flight altitudes focuses on: determining the bathymetry of a portion of Otamiri River (25 Ha) using standard echo sounding procedure; conducting UAS imaging flights on two altitudes over the same portion of Otamiri River in Owerri Imo State; retrieving the bathymetry of the riverbed from the images of the two flights by applying Multiple Linear Regression (MLR) algorithm based on optimal band ratio analysis (OBRA). Ground controls and check points were established with Static and RTK GNSS observations. The images were acquired with 1-Inch CMOS effective 20 megapixels sensor at flight altitudes of 90 m and 150 m with 50% as forward and lateral overlap respectively. The images were processed and georectified with ground control points (GCPs) using Agisoft Photo Scan software. MLR model was calibrated with a fraction of echo sounder depths and the corresponding log-band ratios. The UAS-derived depths were validated statistically by comparing with echo sounder results to determine mean absolute error (MAE), root mean square error (RMSE) and coefficient of determination ( $R^2$ ). The MAE and RMSE (0.27 m and 0.31 m; 0.40 m and 0.48 m) were obtained at 90 m and 150 m flights respectively. The MAE and RMSE increase as the flight height was increased from 90 m to 150 m. Admit other factors, the difference is mainly due to changing flight height. Hence, drone data acquisition should be conducted at lowest possible altitude to achieve finer results.

**Keywords:** *Multiple Linear Regression (MLR) Model, Unmanned Aerial System (UAS),*

*Multispectral Imagery, Bathymetry, Flight Altitude.*



## 1.0 INTRODUCTION

Coastal areas are dynamic and rapidly changing environments at the global scale. Such changes are strongly induced by anthropogenic pressure in synergy with natural coastal processes and changes in global climate [7]. Coastal zones are amongst the most populated areas in the world, with the presence of intensive economic development. At present, approximately 44% of the global human population lives within 150km of the coastal zones [7] and around 10% lives in areas that are less than 10m above sea level [8]. Consequently, there is need for frequent, adequate, quick and up-to- date detailed bathymetry to comprehend the evolution of coastal zones, monitoring, evaluation, coastal flooding studies and forecast, navigation, mapping and monitoring of benthic habits, dredging planning, and coastal management in general [7].

Bathymetry is conventionally acquired via shipboard echo sounding which is usually very expensive, labor-intensive added with inability to access remote or unnavigable areas. But, nowadays, remote sensing methods, such as space-borne or air-borne imaging or lidar have been employed in determining water depth, hence offsetting the setbacks associated with the conventional approaches. The advent of satellite radar altimetry measurement proved worthy alternative solution but provides bathymetric details at a coarser spatial resolution [2]; [8]; [10]; [11].

Nowadays, the use of UAS technology for bathymetry retrieval and other environmental applications has become a norm in the contemporary scientific environment. UAS-derived bathymetry results are more accurate than Satellite derived bathymetry because of the higher image details and does not required atmospheric corrections procedure.



Numerous research works exploring UAS technology in topographic mapping and bathymetry retrieval with promising results have been documented, few of which include; UAS photogrammetry enables précised topographic mapping and the accuracy can be evaluated as a function of changing flight height [13]. Aerial photos of drones coupled with World view -2 satellite sensor permits comparative analysis of strength of various models of bathymetry retrieval [8]. Integration of light weight acoustic sonars with UAV allows for rapid characterization of inaccessible waterbodies and could fill the gap between conventional and remote sensing methods [1]. Accurate digital surface model (DSM) of river channel is an essential tool for flood management and control [14], while points cloud data acquired by optical sensor on board UAV can be used in combination with the profile based data of hydroacoustic sensor to produce a bathymetry chart extending to the boundary of shoreline [5]. With application of geographically weighted regression (GWR) and multiple linear regression (MLR) models, bathymetry information is directly obtained from RGB images of drones acquired in raw digital number without any further conversion process [4]; [15]. Thus, in line with the current research efforts to explore the full potentials of this novel technology and the design of reliable standardized data acquisition process, there is need to assess the reliability of bathymetric information retrieved from UAS-multispectral imageries at different altitudes to guide the end users on the level of trust to be reposed on bathymetry deliverables from such methodology. Hence, investigating the altitude-dependent accuracy of depths derived by colour ratio from UAS multispectral imageries necessitates this study.



## 2.0 THE STUDY AREA

The waterbody under investigation is a portion of Otamiri River in Federal University of Technology, Owerri, Imo State. Imo State is one of the 36 States in Nigeria with Owerri as its capital. It is located in the South-Eastern region of the Country. It lies geographically between Latitude  $5^{\circ} 14' N$  and  $5^{\circ} 30' N$  and Longitude  $6^{\circ} 57' E$  and  $7^{\circ} 02' E$ . Owerri comprises three local government areas, which include Owerri Municipal, Owerri North and Owerri West. Owerri is bounded by Otamiri River to the East and Nworie River to the West. Otamiri River is the longest and popularly known river in Imo State. It takes its source from Isiuza village in Egbu and flows for 50 km through Owerri Municipal, Nekede, Ihiagwa, and Eziobodo to Emeabiam where it forms confluence with Oranmirinkwa River before emptying into Imo River. It is a non-tidal river and only responds to seasonal change in volume. It gets narrower and broader at some sections throughout its length due to sand mining and encroachment from upland. The surface and bottom current changes in magnitude along the river course because of subsequent changes in channel width and bottom slope. Also, it gets deeper and shallower at some points. Besides other water resources, the river is the chief source of sand and gravels which makes it one of the major sources of income to the bordering communities and the State internally generated revenue (IGR) modalities. The selected portion is about 1.16 km long with average width of 220m and total area of about 25 Ha, and just about 50 m from Otamiri-FUTO Bridge. Its openness to good aerial view and appreciable depth was also a prime consideration.

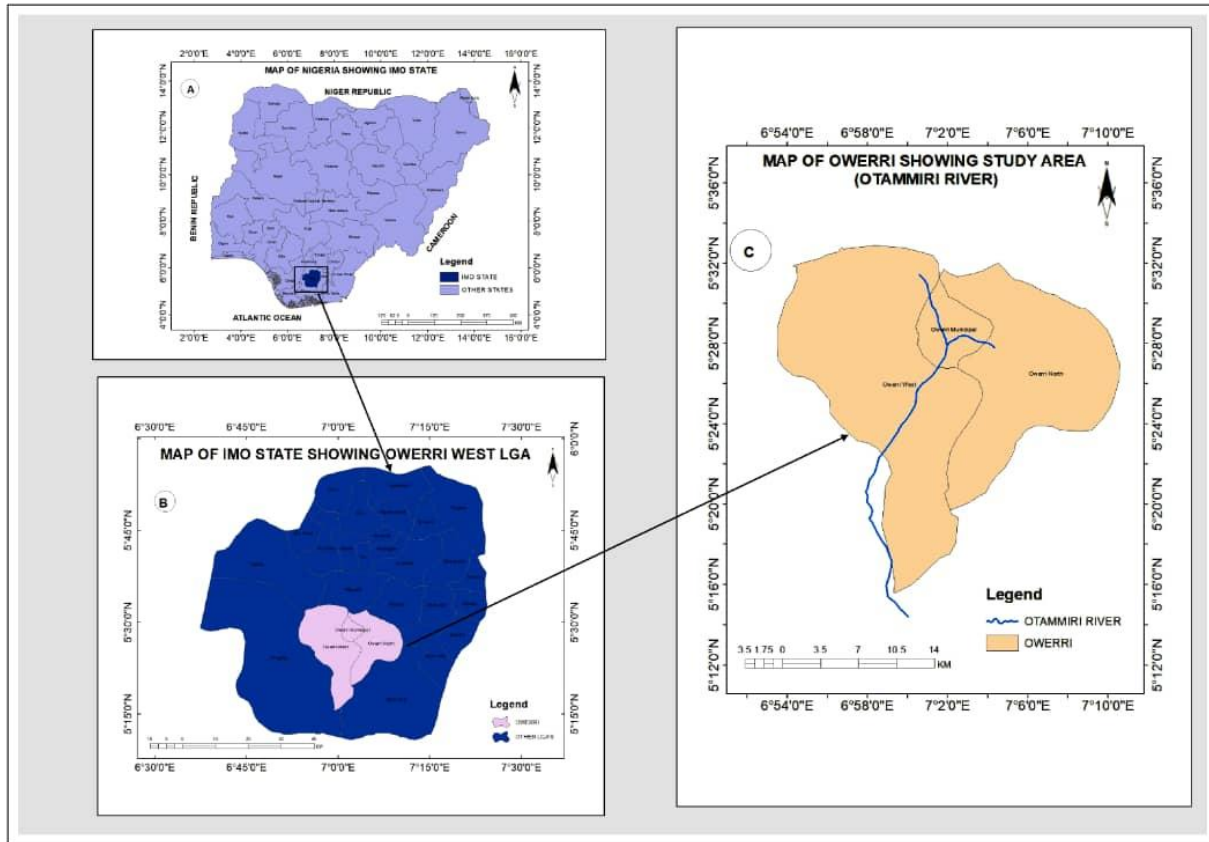


Figure 2.0: Map of the study area.



Figure 2.1: Google earth map showing the study site in red verge.



### 3.0 MATERIALS AND METHODS

#### 3.1 Bathymetric Models

In classical approach based on passive optical image data, the key issue is to estimate depth from multi-spectral or hyper-spectral images, which typically involves establishing a relationship between depth and reflectance at one or more wavelengths. The most common means of calibrating such a relation is to link georeferenced image pixels to field-based depth observations. Bathymetric algorithms can be grouped into two categories; empirical models, which use direct observations of water depth to calibrate reflectance-to-depth relationship, and physics-based inversion models that use radiative transfer models to solve for water depth without in-situ calibration data. Empirical models include; Log-linear model of Lyzenga, Log-ratio model of Stumpf, Optimal band ratio of Legleiter, Multiple Linear Regression (MLR) model, Geographically Weighted Regression (GWR), among others. Physics-based inversion models include; Cluster Based Regression (CBR), Support Vector Regression (SVR), Random Forest Regression (RFR) and others.

Bathymetric algorithms are generally developed from the fundamental principle that light is attenuated exponentially with depth according to Beer Lambert. The equation of relation is expressed by Beer's Law as [12]:

$$L(z) = L(0)\exp(-kz) \quad (3.0)$$

Where,  $k$  is the attenuation coefficient and  $z$  is the depth.



### 3.1.1 Multiple Linear Regression (MLR) Model:

Multiple linear regression model is a statistical model that estimates the relationship between a quantitative dependent variable and two or more independent variable. MLR model is employed in remote sensing because of its ability to model spectral relationship between predictor and measured variables. MLR model exists in two spectral architectures which include;

(i) the structure utilizing the natural logarithmic values of all the three bands of RGB imagery and their respective coefficients with a shared intercept or bias, and in-situ depths for bathymetry inversion. This is described as follows [15].

$$h = a_0 + a_1 \ln(\text{DNR}) + a_2 \ln(\text{DNG}) + a_3 \ln(\text{DNB}) \quad (3.1)$$

Where,  $h$  = estimated depth (m),  $a_0$  = intercept or bias, DNR, DNG, DNB are digital numbers for spectral bands Red, Green and Blue respectively,  $a_1, a_2, a_3$  are regression coefficients,  $\ln$  is the notation for natural logarithms, and

(ii) the structure that incorporates optimal band ratio analysis (OBRA) of Legleiter or principal component analysis (PCA) together with real survey depths to infer the bathymetry of the study area. This is expressed as follows [4].

$$Z(m) = \alpha \ln(\text{DN}_i / \text{DN}_j) + \beta_0 \quad (3.2)$$

Where,  $Z$  = estimated depth (m),  $\alpha$  = regression coefficient,  $i$  and  $j$  are any of the bands of RGB imagery,  $\text{DN}$  = digital number,  $\beta_0$  = intercept or bias.

The model parameters are determined by minimizing the sum of square errors expressed as [4]



$$SSE = \sum_{i=1}^n (h_i - \hat{h}_i)^2 \quad (3.3)$$

Where,  $h_i$  = predicted depth,  $\hat{h}_i$  = measured depth,  $i$  = number of observations, SSE = sum of square errors

Majority of bathymetric algorithms required multispectral or hyperspectral imageries acquired in specific wavelength intervals as inputs, or the image data acquired in raw digital numbers be converted to a common physical scale based on the known reflectance measurements. Hence, the two most widely applicable models to image data in digital numbers format (or RGB) channels are Geographically Weighted Regression (GWR) and Multiple Linear Regression (MLR) models. Though the accuracy of MLR model in bathymetry retrieval weighs slightly below GWR model, it is often preferred over the former in most cases because it is quite simple to execute and requires only two tunable parameters to scale the relative depths to the actual depths. For précised bathymetry retrieval using MLR model, colour or band ratio transformation remain essential. Colour/band ratio can sufficiently compensate for bottom albedo which is a major drawback of single/linear band combinations. Through principal component analysis (PCA), 6 six bands ratios; DNR/DNG, DNR/DNB, DNG/DNR, DNG/DNB, DNB/DNG, and DNB/DNR (3 main ratios and 3 reciprocals) are examined in the RGB image. Where DNR, DNG and DNB are digital number of Red, Green and Blue bands of RGB image respectively. The ratio with the highest component score is chosen as the optimal colour ratio. The natural log-transform of the bands ratios are regarded as the appropriate estimators of water depths [6]. Thus, the natural logarithmic values of the optimal colour/band ratio and the corresponding in-situ depths are used to estimate the model parameters through multiple regression methods. The calibrated model can then be used for



bathymetry inversion. Therefore, the present study employs MLR model based on OBRA or PCA principles for bathymetry inversion.

## 3.2 Data Acquisition

### 3.2.1 Control Establishment for Echo Sounder Survey and UAS Flight

Prior to digital echo sounder survey and UAS flight, two sets of controls were established on the river bank. First, with 1 hour static GNSS observations using Tarsus dual frequency GPS. These controls were used as references for echo sounder determined RTK coordinates of the depth points. For UAS flight, a set of ground check points (GCPs) were uniformly spaced within the study area and their coordinates determined with 1 minute RTK GNSS observations. These set of controls were used for georeferencing of UAS acquired images. Markers made of flex with dimension 1 m by 1 m and high contrast paint with précised arrow tip were placed on each of the GCPs with the tip of the arrow made to coincide exactly with the coordinated points. These markers were used to align the aerial photographs during image processing.



**Figure 3.1:** Spatial locations of two of the ground control markers, PL026 (A) and PL011 (B).

### 3.2.2 Conventional Bathymetric Survey with Digital Echo Sounder

Upon the design of sounding plan and control establishment, the parameters of South digital single-beam echo sounder (Model: SDE-28S<sup>+</sup>) operating at pulse repetition frequency of 280 KHz



[www.journals.unizik.edu.ng/jsis](http://www.journals.unizik.edu.ng/jsis)

including coordinates transformation parameters were set. Configuration and instrumentation were strictly carried out for maximum operational efficiency. The South echo sounder proprietary software (Power-Navs) was launched and the survey vessel was directed along the pre-planned sounding line at an average cruising speed of 0.0049 Knot (0.009Km/h) and the fixes logged-in immediately. Depths were determined in instantaneous mode at the fix interval of 3000 seconds (7.5 m). The heading on each sounding line was maintained following the bearing displayed on the echo sounder monitoring unit. The sounding operation was conducted in a systematic manner following the pre-planned sounding lines. In all, a total of twenty eight (23) cross lines and one central profile were adequately covered. The echo sounder was interfaced with Real Time Kinematic (RTK) GPS sensor for collecting attitude-corrected bathymetry points at 2.5Hertz rate. The RTK measurements provide high spatial accuracy (<5 cm) sufficiently enough for point to point comparison of depths estimated from drone-based imagery with a pixel resolution of a few centimetres. The echo sounder transducer was deployed at the stern of the vessel and the GPS receiver was mounted directly on the transducer pole a zero offset. The transducer draft of 0.5 m was measured and inputted into the software during instrument configuration for automatic correction of the fixed error. The minimum depth 0.56m upstream around the north-eastern part of the area and maximum depth of 9.44 m downstream around the south-eastern part was recorded.



The average depth of the area measured was 5.54 m, and a total of 2542 bathymetry points were acquired.

**F**

**Figure 3.2:** Shows sailing of the survey vessel after configuration (A), instantaneous position of

**A** berthing of the vessel after operations (C).

### 3.2.3 Unmanned Aerial System (UAS) Flight

The Unmanned Aerial System (UAS) used in this study comprises off-the-shelf DJI Phantom 4 Professional quad copter spreading wings UAV of weight 2 kg equipped with multispectral camera acquiring images in three (3) spectral bands of electromagnetic spectrum, and DJI Go 4 flight controller, Model: GL300L, manufactured by SZ DJI Technology CO. LTD., China. The camera lens of the UAV has a field of view (FOV) of 84°, and a focal length of 8.8 mm/24 mm (35 mm format equivalent). The gimbal has a controllable range of -90° to +30° and a maximum controllable angular speed of about 90°/s. The UAV system is equipped with positioning system that can track both GPS and GLONASS satellites with vertical and planimetric accuracy range of



$\pm 0.5m$  and  $\pm 1.5m$  respectively. As a consequence of the battery limitations, the UAV has a maximum flight time of approximately 30 minutes.



[www.journals.unizik.edu.ng/jsis](http://www.journals.unizik.edu.ng/jsis)

Following the preparation of the flight plan and the measurement of the GCPs, the parameters of the UAV were set to default in accordance with standard recommendations. The drone was checked to ensure it was in optimum condition. The flight operation was conducted in a systematic manner based on pre-planned flight paths to ensure perfect coverage and maximum efficiency. During the flight, the UAV was monitored to ensure it was within the range of visual contact as any other aerial obstacle and related accident must be avoided. Weather was as well monitored to ensure it was in optimum condition for quality data acquisition as strong winds and adverse conditions affect smooth operation of drones. Precisely, once the UAV had passed its first strip or flight path (otherwise waypoint), the next strip was initiated. Consequently, the drone acquired images following the pre-programmed flight strips. After passing the last strip on the flight lines, the UAV terminated its flight mission and initiated a normal landing process as programmed whilst landing at the take-off point. The images were acquired at the flight altitude of 90 m and 150 m with 50% as fore and side overlaps respectively. The two flights took about 15 to 20 minutes to cover the entire area of study and a total of 371 and 172 images were captured. The UAV flight was conducted concurrently with bathymetric survey to eliminate any bias that may arise as a result of morphological variations due to the gap of time between the bathymetric survey and image acquisition.



A

B.

**Figure 3.3:** UAV take-off point (A) and landing (B) at the project site.

### 3.3 Data Processing

#### 3.3.1 Processing of GNSS Observations

Upon the completion of static GNSS observations, the GNSS receivers were taken to the laboratory for data downloading and post-processing. The receivers were connected to computer and the data was downloaded and stored in a newly created folder. Trimble Business Centre (TBC-Version 2.50) software was launched and the project settings including definition of coordinate system/datum to WGS84 UTM Zone 32N were set. The downloaded data was then inputted. The baseline processing was carried out and the report of the post-processed coordinates was generated and saved in CSV (Comma Separated Variable) file format.

#### 3.3.2 Processing of Echo Sounder Data

After the completion of the bathymetric survey, the echo sounder display/monitoring unit was taken to the laboratory where it was connected to laptop and the data was downloaded and stored in a notepad format. Microsoft excel (Version 10.0) was launched and the data was imported. Here,



all the acquired data with their attributes were display on the table in rows and columns. The data were trimmed by removing rows and columns containing unnecessary information.

### 3.3.3 Processing of Unmanned Aerial System (UAS) images

The completion of photogrammetric task was immediately proceeded with downloading and processing of raw images captured by the UAV. The data storage device was retrieved from the UAV and inserted into laptop where the raw aerial photos were downloaded and stored in a notepad format. The parameters of the Agisoft photoscan software including definition to appropriate coordinates datum/transformation were set in this case the NTM MIDBELT using Chevron Nigeria Limited (CNL) transformation parameters. The first approach to processing involves image alignment and geo-rectification with GCPs, thereby enabling determination of precise position of each GCPs using their position in the original 2D images. The generated products include Digital Elevation Model (DEM) and Orthophoto of the study area.

The spatial accuracies of XYZ-coordinates of the ground check points and their relative position in the images were computed using the following equations [3];

$$\text{RMSE} = \sqrt{\frac{\sum_{i=1}^n (N_m - N_e)^2}{n}} \quad (3.4)$$

Where,  $N_m$ = measured values,  $N_e$ = estimated values,  $n$ = total no. of points,  $i$ = counter.

The planimetric/horizontal  $\text{RMSE}_H$  was computed as follows;

$$\text{RMSE}_H = \sqrt{\frac{\sum_{i=1}^n (X_m - X_e)^2 + (Y_m - Y_e)^2}{n}} \quad (3.5)$$

Equation (2.14) can be explicitly expressed as;



$$RMSE_X = \sqrt{\frac{\sum_{i=1}^n (X_m - X_e)^2}{n}} \quad (3.6)$$

$$RMSE_Y = \sqrt{\frac{\sum_{i=1}^n (Y_m - Y_e)^2}{n}} \quad (3.7)$$

Then, the vertical RMSE (Z-component) is expressed as;

$$RMSE_Z = \sqrt{\frac{\sum_{i=1}^n (Z_m - Z_e)^2}{n}} \quad (3.8)$$

Where:

$X_m$  = the measured easting coordinate of the GCPs,

$X_e$  = the estimated easting coordinate of the orthophoto check point,

$Y_m$  = the measured northing coordinate of the GCPs,

$Y_e$  = the estimated northing coordinate of the orthophoto check point,

$Z_m$  = the measured height of the GCPs,

$Z_e$  = the estimated height of the orthophoto check point,

$n$  = the number of check points.

**Table 3.1:** Presents spatial accuracy of the GCPs and their corresponding points in the orthophoto at 90 m flight height.

Label	X-error(mm)	Y error(mm)	Z error(mm)	Total(mm)	Image(pix)
PL 01	-0.237128	-0.121640	-0.0742548	0.276658	0.006 (6)
PL 02	0.0958617	0.1309180	-0.3332420	0.370647	0.005 (8)
<b>Total</b>	<b>0.180858</b>	<b>0.126364</b>	<b>0.241417</b>	<b>0.327047</b>	<b>0.005</b>

**Table 3.2:** Presents spatial accuracy of the GCPs and their corresponding points in the orthophoto at 150m flight height.



Label	X-error(mm)	Y error(mm)	Z error(mm)	Total(mm)	Image(pix)
PL 01	-0.237128	-0.121640	-0.0742548	0.276658	0.006 (6)
PL 02	0.0958617	0.1309180	-0.3332420	0.370647	0.005 (8)
<b>Total</b>	<b>0.180858</b>	<b>0.126364</b>	<b>0.241417</b>	<b>0.327047</b>	<b>0.005</b>

### 3.4 Bathymetry Retrieval Using MLR Model:

In this study, multiple linear regression (MLR) model based on optimal band ratio analysis (OBRA) or principal component analysis (PCA) was adopted for bathymetry derivation because of its simple and intuitive nature, and requires only two tunable parameters which can easily be determined by multiple regression methods. Also, the image data employed for this research were acquired in three (3) visible bands (RGB) of electromagnetic radiation. The spectral architecture of OBRA or PCA incorporated MLR model is mathematically expressed by equations (3.1) and (3.2) as earlier stated.

For bathymetry inversion model calibration, a fraction of echo sounding points were used as reference depths. These points were randomly selected in the study area. The generated orthophoto was exported to ArcGIS environment upon which ground-truthing depth samples were overlaid and their corresponding pixels values extracted using the module “extract multi values to points” under Spatial Analyst Tools in ArcGIS domain. OBRA or PCA was used to extract optimal band ratio that is most suitable for the water conditions of the study area. The six band ratios (DNR/DNG, DNR/DNB, DNG/DNR, DNG/DNB, DNB/DNG, and DNB/DNR) were examined in the RGB image. Through the principal component analysis (PCA), the ratio of digital number Green band (DNG) to digital number Red band (DNR) had the highest component score (or  $R^2 = 0.8781$ ). Therefore, the natural logarithmic values ( $\text{Ln}(\text{DNG}/\text{DNR})$ ) of DNG and DNR ratios and



their corresponding in-situ depth samples were used as predictor and objective variables to estimate the model parameters. Consequently, the following equations were generated for depth estimation process;

$$Z(m) = 47.2948 * \ln(DNG_i / DNR_j) + 0.1421 \quad (3.9)$$

Where,  $Z = y =$  estimated depth,  $\alpha = 47.294$  (the slope),  $x =$  independent variable ( $\ln(DNG_i / DNR_j)$ ),  $\beta_0 = 0.1421$  (the intercept or bias). Equation (3.9) is the calibrated or depth estimation equation for 90m orthophoto.

$$Z(m) = 37.446 * \ln(DNG_i / DNR_j) + 0.757 \quad (3.10)$$

Where,  $\alpha = 37.446$  (the slope),  $\beta_0 = 0.757$  (the intercept or bias),  $x =$  independent variable ( $\ln(DNG_i / DNR_j)$ ). Equation (3.10) is the calibrated/depth estimation equation for 150m orthophoto.

The calibrated model/equation for each flight was tested on about 1513 real bathymetry points to verify its reliability for bathymetry inversion in the study area.

## 4.0 RESULTS AND DISCUSSION

### 4.1 Bathymetry Inversion Results Validation and Accuracy Assessment:

UAS-derived bathymetry was validated with about 414 real dataset in order to determine mean absolute error (MAE), root mean squared error (RMSE) and coefficient of determination ( $R^2$ ).

MAE, RMSE and  $R^2$  were computed using equations 4.1, 4.2 and 4.3 [15].

$$MAE = \frac{1}{n} \sum_{i=1}^n |Z_i - H_i| \quad (4.1)$$



$$RMSE = \sqrt{\frac{\sum_{i=1}^n (Z_i - H_i)^2}{n}} \tag{4.2}$$

$$R^2 = 1 - \frac{\sum_{i=1}^n (Z_i - H_i)^2}{\sum_{i=1}^n (Z_i - \hat{Z}_i)^2} \tag{4.3}$$

Where  $Z_i$  and  $H_i$  denote the real water depth and estimated depth of the test point  $i$  respectively,  $\hat{Z}$  denotes the mean value of  $n$  real water depths, and  $n$  is the number of test points.

Scatter plot of derived versus measured field depths were executed to examine the degree of correspondence or relationship and pattern of data dispersion around regression line/line of best-fit.

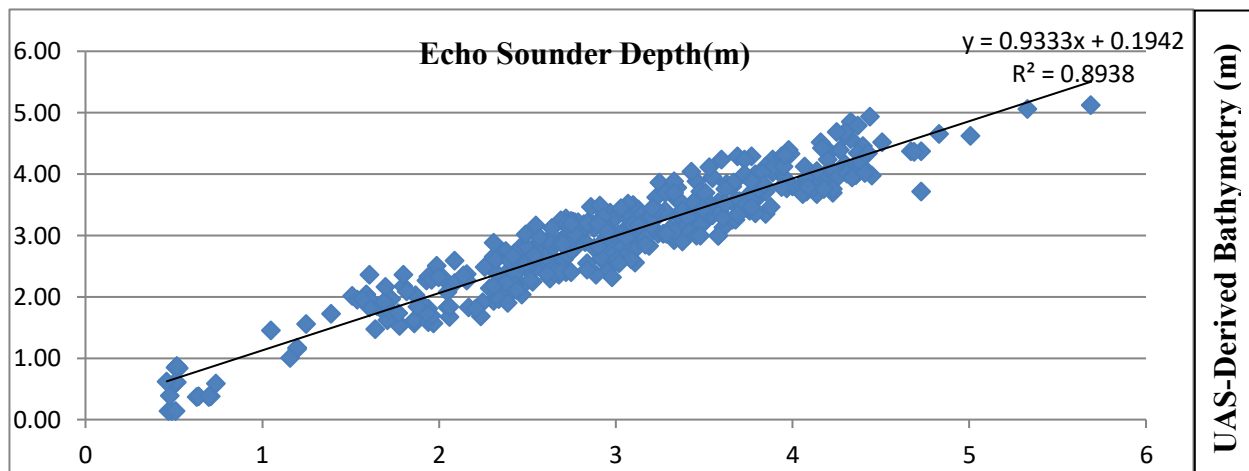


**Figure 4.1:** Scatter plot of UAS-Derived Bathymetry versus Echo Sounder depth with prediction equation and coefficient of determination ( $R^2$ ) for 90m orthophoto.

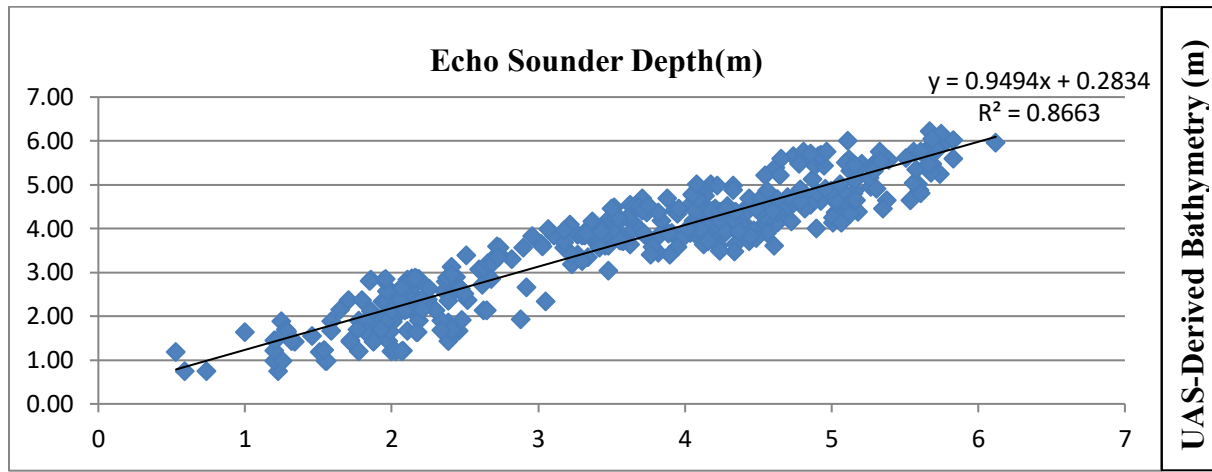


**Figure 4.2:** Scatter plot of UAS-Derived Bathymetry versus Echo Sounder depths with prediction equation and coefficient of determination ( $R^2$ ) for 150m orthophoto.

UAS-derived bathymetry fits the riverbed relatively well. Scatter plots of UAS-derived bathymetries (UDB) versus real survey depths depict an even points dispersion for the two flights. The higher coefficient of determination indicates better goodness of fit of UDB.

The results of accuracy analysis of the observations retrieved by the sonar and UAS-Derived Bathymetries (UDB) are presented in Table 4.1.

**Table 4.1:** Comparison of accuracy analysis of measured field depth and derived bathymetry.

Operations	Flight Altitude (m)	Validation points	Depth range (m)	MAE (m)	RMSE (m)	$R^2$
Sonar depth-	90	414	0-6.5	0.2695	0.3114	0.8938
Derived depth	150	414		0.3953	0.4828	0.8663

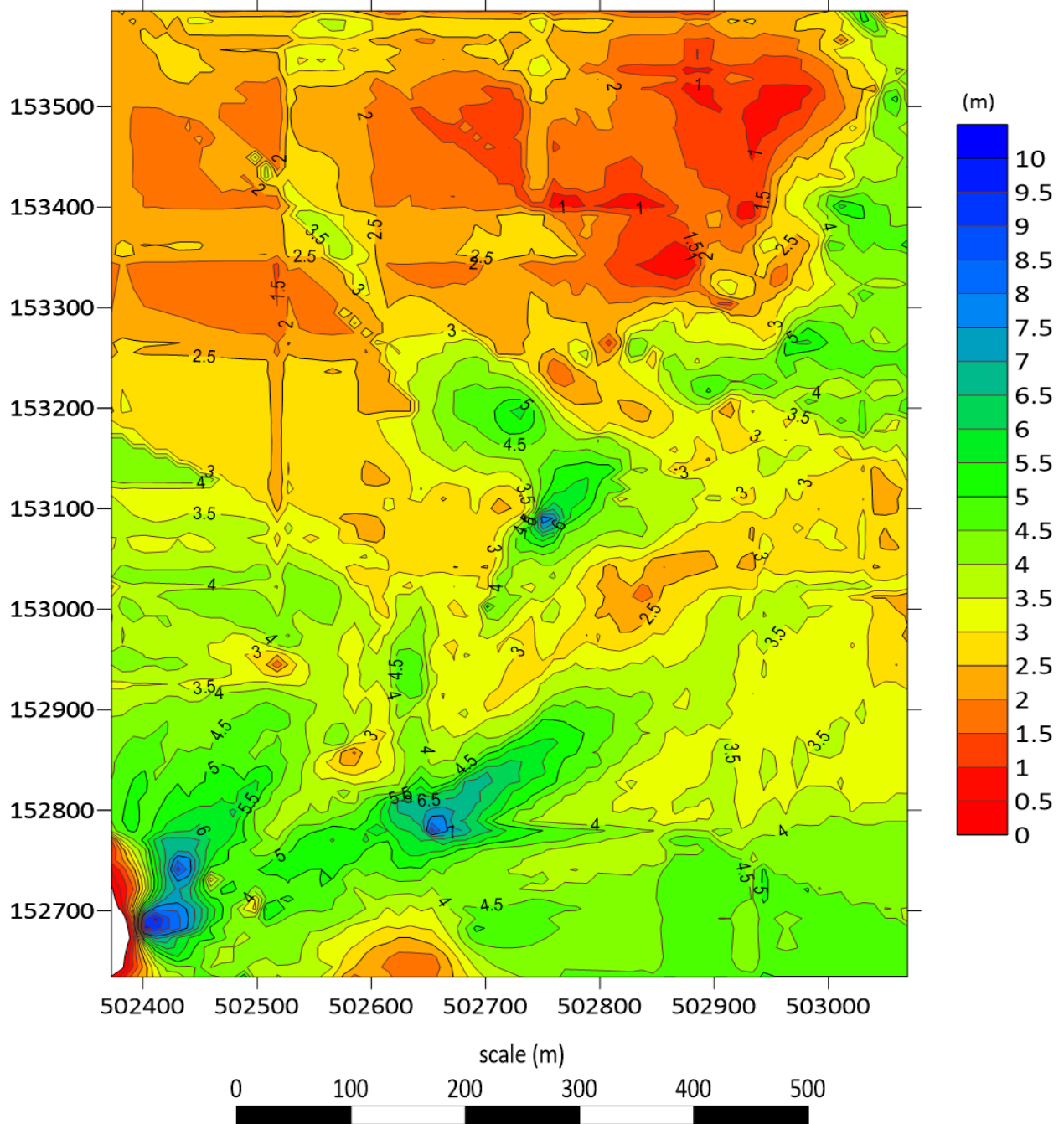
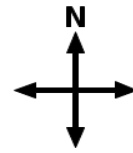


Form the table, the root mean square error achieved at 90 m flight is less than that of 150 m flight. The absolute difference of root mean square error (RMSE) value of bathymetries obtained at 90m and 150m flights is 0.1714 m. This difference appears insignificant in value. However, it may become more pronounced as the interval between successive flight altitude increases. Some prevailing factors such as image matching/processing mechanism and field uncertainties can degrade the accuracy of the final results. However, the results of accuracy analysis of this study shows that variation in accuracies of bathymetries achieved for each flight is most likely due to changing flight heights.

A non-metric analysis, otherwise qualitative analysis was carried to ascertain the spatial relativity of the real world phenomenon represented by the products of the two techniques of data acquisition employed in this study.

For this study, qualitative analysis was carried out by visual comparison of the quality of the bathymetry maps produced from the two different methodologies of data acquisition adopted in this research. Figure 4.3 A and B shows orthophotos from 90m and 150m flights respectively, while figure 4.4, 4.5 and 4.6 depict bathymetry maps constructed from sonar observations and bathymetry algorithms.





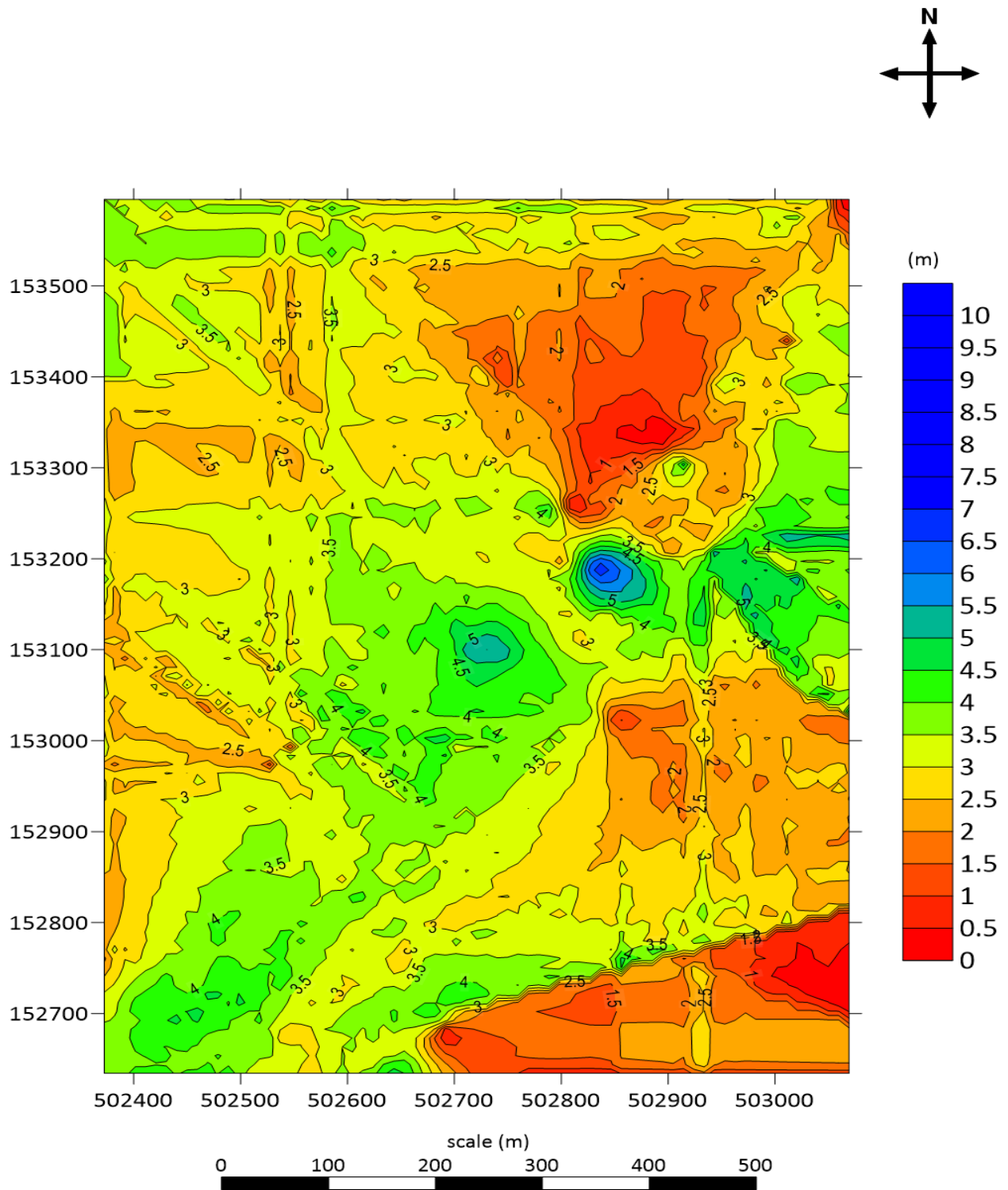


**Figure 4.5:** Bathymetry map of UAS-derived bathymetry at 90m flight.

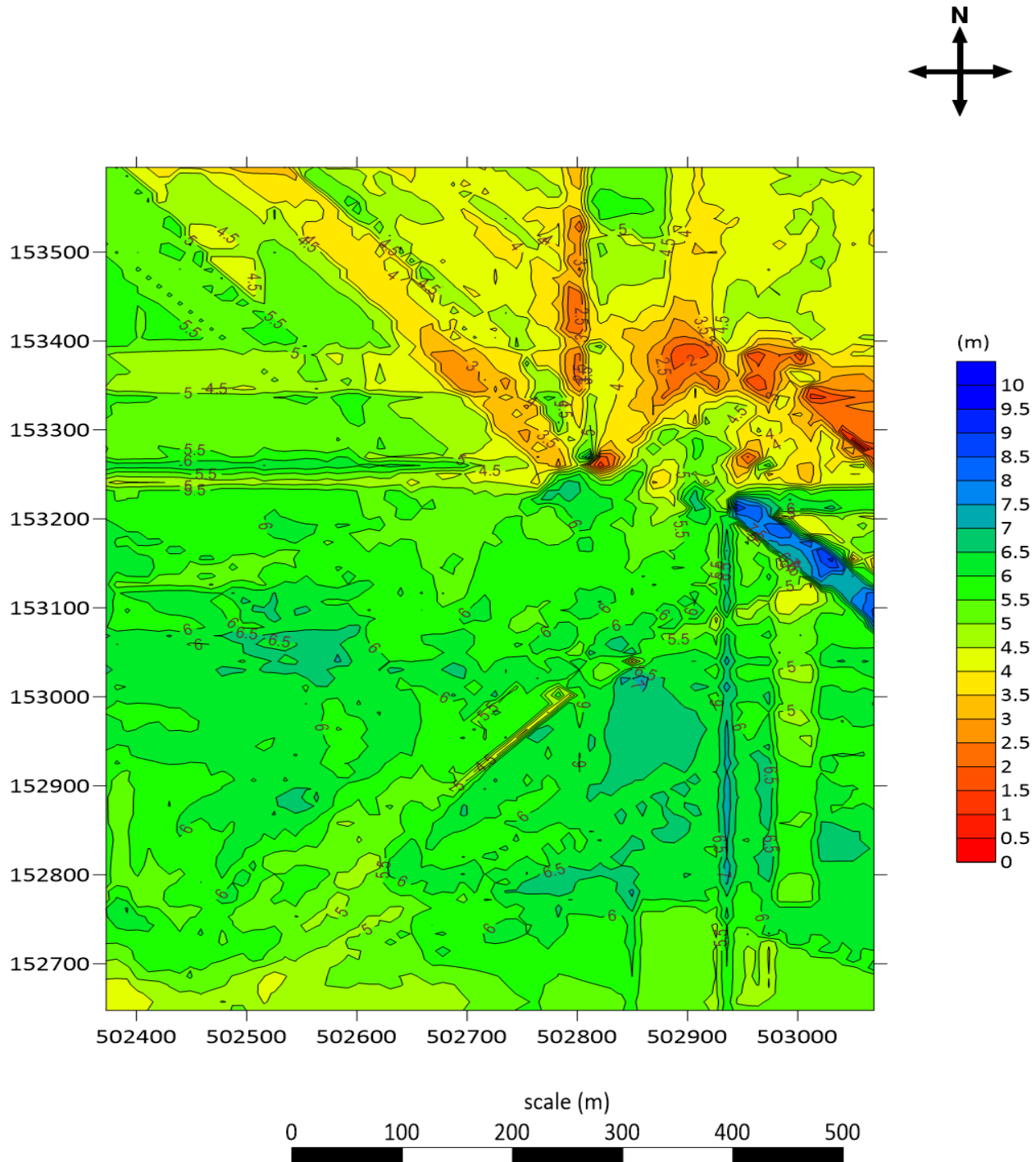




**Figure 4.6:** Bathymetry map of UAS-derived bathymetry at 150m flight.

Depths are portrayed in code of colours, where deep red indicates the shallowest regions and deep blue represents the deepest portions. The scale bar and the depths legend in each figure are graduated in metres. The depth contour interval is 0.5m.

## 5.0 Conclusion:

The study has successfully demonstrated the impacts of changing flight altitude on the accuracy and precision of depths estimated from passive or active optical systems, particularly, UAS imageries. The absolute difference of root mean square error (RMSE) value of bathymetries obtained at 90m and 150m flights is 0.1714 m (Table 4.1). This difference only manifests in decimetric precision level and appears insignificant in value. However, it may become more pronounced as the interval between successive flight altitude increases. Some prevailing factors such as image matching/processing mechanism and field uncertainties can degrade the accuracy of the final results. However, the results of accuracy analysis of this study shows that variation in accuracies of bathymetries achieved for each flight is most likely due to changing flight heights.

Radiometrically, the observed spatial variation in the response of the selected band ratio over depths could result from a number of factors such as varying bottom substrates (soft mud, gravels, sand, submerged vegetation and grass), variation in optics and change in illumination. As the depth of the survey increased beyond 6.5 m, the underestimation of depths by the model becomes more pronounced as the direct consequence of the attenuation of electromagnetic radiation efficiency due to absorption in the water column. This failure represents a fundamental limitation of depth



estimation from optical systems regardless of the methods [12]. The overestimation and underestimation of depths was also observed at some points in the shallow regions of the study area which may probably be due to non-uniform spatial distribution of the bottom materials. Based on the findings of this research, for the intent of achieving a more finer results in bathymetry retrieval and topographic mapping, the study propose that all topographic and bathymetric data acquisition with drones be conducted at the lowest possible height considering the size of the study area, presence of some sorts of aerial obstacles and the local flight permissions. The use of other bathymetric algorithms to further investigate the results of this study is necessary. The study can as well be conducted in other coastal and inland waterbodies with varied characteristics to further confirm the findings of this paper.

## REFERENCES

- [1] Bandini, F.; Olesen, D.; Jakobsen, J.; Kittel, C.; Wang, S.; Garcia M. and Bauer-Gottwein, P. (2018). Bathymetry observations of Inland Water Bodies using tethered single-beam sonar controlled by an Unmanned Aerial Vehicle. *International Journal of Hydrology and Earth System Sciences*, 22, 4165–4181.
- [2] Calmant, S., Seyler, F., and Cretaux, J. (2009). Monitoring continental surface waters by satellite altimetry. *Surveys in Geophysics*, 29(4), 247-269.
- [3] Gbopa, A. O., Ayodele, E. G., Okolie, C. J., Akinwumi, O. A., and Iheaturu, C. J. (2021). Unmanned aerial system for three-dimensional mapping and change detection analysis. *Geomatics and Environmental Engineering*, 15(1). <https://doi.org/10.7494/geom.2021.15.1.41>. 16 September, 2023.
- [4] Jun, S. K.; Donghae, B.; Il, W. S.; Jachyun, S. (2019). Retrieving shallow stream bathymetry from UAV-Assisted RGB imagery using a geospatial regression method. *Geomorphology*, 341, 102-114. <https://doi.org/10.1016/j.geomorph.2019.05.016>. 9, February, 2024.



- [5] Lubczonek, J., Kazimierski, W., Zaniewicz, G., Lacka, M. (2022). Methodology for combining data acquired by unmanned surface and aerial vehicles to create digital bathymetric models in shallow and ultra-shallow waters. *Remote Sens*, 14(105).
- [6] Legleiter, C. J. (2012). Remote measurement of river morphology via fusion of lidar bathymetry topography and spectrally based bathymetry. *Earth Surf. Proc. Land.*, 37, 499-518.  
<https://doi.org/10.1002/esp.2262>, 24 August, 2022.
- [7] Muzirafuti, A., Barreca, G., Crupi, A., Faina, G., Paltrinieri, D., Lanza, S., Randazzo, G. (2020). The contribution of multispectral satellite image to shallow water bathymetry mapping on the coast of Misano Adriatico, Italy. *International Journal of Marine Science Engineering*, 8(126).
- [8] Rossi L.; Mammi, I.; Pelliccia, F. (2020). UAV-derived multispectral bathymetry. *International Journal of Remote Sensing*, 12, 3897.
- [9] Sandwell, D. T.; Muller, R. D., Smith, W. H. F.; Garcia, E. and Francis, R. (2014). New global marine gravity model from CryoSat-2 and Jason-1. Reveals buried tectonic structure. *Science*, 346(6205), 65–67.
- [10] Sandwell, D. T.; Smith, W. H. F.; Gille, S.; Kappel, E.; Jayne, S.; Soofi, K. *et al.* (2006). Bathymetry from space: Rationale and requirements for a new high-resolution altimetry scission. *Comptes Rendus Geoscience*, 338(14), 1049–1062.
- [11] Smith, W. H. F. and Sandwell, D. T. (2004). Conventional bathymetry from space and geodetic altimetry. *Applied Optics*, 38(18), 3831–3843.
- [12] Stumpf, R. P., Holderied, K., and Sinclair, M. (2003). Determination of water depth with high resolution satellite imagery over variable bottom types. *Limnology and Oceanography*, 48, 547-556. [https://doi.org/10.4319/lo.2003.48.1\\_part\\_2.0547](https://doi.org/10.4319/lo.2003.48.1_part_2.0547). 13 July, 2022.
- [13] Udin, W. S. and Ahmad, A. (2014). Assessment of photogrammetric mapping accuracy based on variation in flight altitudes using unmanned aerial vehicle. *Earth and Environmental Science*, 18(1). Doi:10.1088/1755-1315/18/1/012027. 20 March, 2022.



- [14] Watanabe, Y. and Kawahara, Y. (2016). UAV Photogrammetry for monitoring changes in river topography and vegetation. 12<sup>th</sup> *International Conference on Hydroinformatics, HIC2016. Procedia Engineering 154*(16) 317–325.
- [15] Wang, J.; Chen, M.; Zhu, W.; Hu, L.; Wang, Y. (2022). Combined approach for retrieving bathymetry from aerials stereo RGB imagery. *Remote Sens.* 2022, *14*, 760. <https://doi.org/10.3390/rs14030760>. 25 April, 2024.